Available online at www.sciencedirect.com

jmr&t Journal of Materials Research and Technology

journal homepage: www.elsevier.com/locate/jmrt

Original Article

Energy consumption, wear and corrosion of PEO coatings on preanodized Al alloy: the influence of current and frequency

M. Mohedano [a,*], E. Lopez [a], B. Mingo [b], S. Moon [c], E. Matykina [a], R. Arrabal [a]

[a] Departamento de Ingeniería Química y de Materiales, Facultad de Ciencias Químicas, Universidad Complutense de Madrid, 28040, Spain

[b] Department of Materials, University of Manchester, Oxford Road, Manchester, M13 9PL, UK

[c] Surface Engineering Division, Korea Institute of Materials Science (KIMS), South Korea

ARTICLE INFO

Article history:
Received 12 July 2022
Accepted 13 October 2022
Available online 18 October 2022

Keywords:
Anodizing
Plasma electrolytic oxidation
Aluminum

ABSTRACT

The influence of current and frequency on energy consumption of plasma electrolytic oxidation (PEO) of a commercial aluminium alloy pre-treated by conventional anodizing in sulphuric acid has been investigated. The combination of a 20-μm thick precursor anodic porous film, high current (500 mA cm^{-2}) and frequency (400 Hz) during PEO enables up to 76% energy savings compared to direct PEO treatment (50 Hz). The time needed to achieve a uniform coating thickness was also reduced from 3350 s to 750 s, for PEO_50 and A + PEO_400, respectively. The wear and corrosion performance of the optimised coatings (400 Hz) were also improved despite the lower thickness of the coatings. Such improvement was mainly attributed to the microstructural refinement associated with high frequency processing and early transaction to the "soft-sparking" regime. The modification of the frequency has a stronger influence on the corrosion response than the presence of the anodic precursor. The best corrosion response was obtained for PEO_400 followed closely by A + PEO_400.

1. Introduction

High energy consumption is currently limiting the application of plasma electrolytic oxidation (PEO) of aluminium alloys to niche applications in high-end technologies such as the aerospace, gas and oil industries, where the excellent range of mechanical, corrosion and wear properties of these coatings can be exploited [1].

During the last years, there has been an increasing number of studies addressing practical approaches in order to increase the energy efficiency of PEO processing and make it economically viable for mass production applications. Examples of these are: i) substitution of DC by AC and bipolar electric signals, with the aim to control the energy and lifetime of microdischarges [2,3]; ii) cell and cathode geometry design [4]; iii) electrolyte additives in the form of complexing agents or nanoparticles [5,6]; and iv) pretreatment by conventional anodizing [5,7–9]. The latter approach, which was first proposed by the authors of the present study, has been shown to save up to 50% depending on the alloy substrate [10].

* Corresponding author.
E-mail address: mmohedan@ucm.es (M. Mohedano).

https://doi.org/10.1016/j.jmrt.2022.10.049

The idea of a precursor film is based on reducing the energy consumption required to achieve the coating thickness that is normally needed to promote the establishment of the so-called "soft sparking" during PEO [8,11]. This regime increases the coating growth rate and facilitates the formation of the intermediate dense layer, which provides the main thermomechanical and tribological properties of PEO coatings in aluminium alloys [7].

Proper adjustment of current and frequency has been shown in the past to be crucial for energy savings in PEO processing of aluminium alloys [3,12]. However, to the best of the authors' knowledge, these parameters have not been studied in a commercial aluminum alloy pretreated by conventional anodizing, which is precisely the main goal of the present study.

Reducing the overall energy consumption of the process should not compromise the performance of the coatings. Several works have shown that modifying the processing parameters such as frequency and current density leads to an improvement of their corrosion and wear performance [13,14], although no information is provided regarding their influence on the energy efficiency. Studies involving the evaluation of the performance and energy efficiency of precursors for PEO are quite limited. In a recently published work by the authors [10], it was reported that the use of anodic precursors on PEO coatings developed using different phosphate based electrolytes improves the energy efficiency up to 66%, although they did not have a significant positive influence on the corrosion performance.

The present work presents several strategies based on optimization of the processing frequency, current density and use of an anodic precursor that allow significant energy saving of the process while simultaneously improving the performance of the developed coatings. The results presented in this work envisage the feasibility of upscaling PEO process for components subjected to corrosive and tribological environments.

2. Methods

2.1. Test materials

2.1.1. Pre-anodizing or precursor film

Rectangular specimens (40 × 20 × 1.5 mm^3) of aluminium alloy 6082 were etched for 30 s in 50 wt% sodium hydroxide solution, desmutted in a 70 wt% nitric acid solution for 30 s, rinsed in distilled water and dried in warm air. Masked specimens (~5 cm^2 working area) were pretreated by conventional anodizing in 24.5 wt% sulphuric acid (20 °C, 50 mA cm^{-2}, 800 s) in order to produce a 20 μm-thick alumina precursor layer.

2.1.2. PEO

PEO treatment was carried out by using a 2 kW EAC-S2000 power supply (ET Systems electronic) with a square electrical signal (+490V/-110V, 50% duty cycle) and an initial ramp of 60 s. Current (rms) and frequency values were set at different values in the range 50–400 Hz and 350–500 mA cm^{-2} respectively. Higher values could not be studied due to power supply design limitations. The rms voltage and current responses were acquired electronically, with a sampling time of 0.1 s, employing a KUSB-3116 Keithley data acquisition card. Instantaneous voltage and current values were monitored and recorded using a 2-channel Tektronix TDS 2012B oscilloscope at 100 MHz sampling rate. The treatment was stopped 600 s after a current drop was observed or when the rms current value decreased to values below 100 mA cm^{-2}, whichever happened first. The electrolyte, comprising 10.5 g L^{-1} sodium silicate (1.39 kg dm^{-3}), 5 g L^{-1} sodium phosphate dodecahydrate and 2.8 g L^{-1} potassium hydroxide, was continuously stirred during the treatment in a 2 L double-walled glass cell with a stainless steel counter electrode and re-circulating water at 20 °C. After PEO treatment, the specimens were rinsed in water and dried in warm air.

2.2. The specific energy consumption

The specific energy consumption of the PEO process (kW h m^{-2}) was calculated by integration (Eq. (1)) of the instantaneous voltage and current waveforms. The data were recorded periodically by the power supply (SM 400AR-8 Systems electronic, 2-channel Tektronix TDS 2012B oscilloscope at 100 MHz sampling rate) at different stages of the treatment: i) first, at 60 s, 120 s and 300 s; ii) then, every 300 s until the drop of the current; iii) at the beginning of the current drop, at 300 s from the current drop and 50 s before the end of the treatment.

$$E_{TOTAL} = \int_{to}^{t} [V\ i] \left[\frac{W\ s}{m^2}\right] dt \quad (1)$$

(V: instantaneous voltage, i: instantaneous current density, t0: the starting point of the experiment, t: the end time of the experiment).

The total energy includes the sum of energy consumed by PEO process and the energy consumed during anodic process when applicable (the energy consumed during conventional anodizing is ~2 kW h m^{-2} to obtain a ~20-μm-thick oxide layer).

2.3. Specimen characterization

Coating cross-sections were prepared following standard metallographic procedures and examined by scanning electron microscopy (SEM) using a JEOL JSM-6400 microscope equipped with Oxford Link energy dispersive X-ray (EDS) microanalysis hardware. Coating thicknesses were measured by the eddy-current method (Isoscope FMP10, Fischer) taking the average of 20 measurements at randomly selected places and later confirmed by SEM examination. Surface roughness was studied with a focus variation optical profilometer with a × 50 lense (Alicona InfiniteFocusSL). Coating hardness was evaluated using an AKASHI MVK-E3 Vickers micro-hardness tester on polished cross sections under a load of 10 g for 20 s. The cited values are the average of ten measurements. Phase composition was examined by X-ray diffraction (XRD) using a Philips X'Pert diffractometer (Cu $K_\alpha = 1.54056$ Å) at a scanning speed of 0.04° per second for a scan range of 2θ from 10° to 80° with an incidence angle of 90° and 2 s/step of counting time.

Image analysis of the microdischarges was carried out on optical images of the specimens obtained at different treatment times (60, 120 and 300 s) using the software ImageJ. To quantify

the microdischage density and area faction, the images were transformed into a 8-bit greyscale and a sharpen filter was used that increases contrast and accentuate details by applying a weighting factor to replace each pixel with a weighted average of the 3 × 3 neighborhood. Finally, an automated segmentation was carried out for the quantification.

2.4. Wear tests

To evaluate the tribological properties of selected coatings, a MT/60/NI tester (MicroTest) was used in dry conditions at room temperature (~21 °C) and ~35% humidity. Tests were performed in ball-on-flat linear reciprocating mode with a stroke length of 10 mm and a maximum sliding distance of 120 m. The coatings served as the plates and the counterpart was a WC ball of 6 mm in diameter and 1800 HV hardness. The normal load was 10 N.

The wear rates (Wr) were estimated dividing the wear volume (Wv) by the normal load applied and total sliding distance. The Wv was measured by high resolution 3D measurements (InfiniteFocusSL, Bruker Alicona) of the worn surfaces and corresponds to volume inside the wear track below the adjacent surface. The final Wr was the average of the three tests per specimen.

To conduct the wear tests, the outer layer of the coatings was removed (about 20 μm) by grinding with a P320 SiC abrasive paper in order to obtain a flat and smooth surface and eliminate the outer part of the PEO coatings.

2.5. Corrosion evaluation

Electrochemical impedance spectroscopy (EIS) measurements were conducted after 1 h of immersion to evaluate the corrosion performance of the selected coatings in naturally-aerated 3.5 wt% NaCl aqueous solution at ~22 °C.

A three-electrode cell connected to a GillAC computer-controlled potentiostat (ACM Instruments) was used. The working area of the specimens was defined as 1 cm^2; the counter and reference electrodes were graphite and silver/silver chloride (Ag/AgCl in 3 M KCl), respectively. A sinusoidal perturbation of 10 mV amplitude in the frequency range of 100 kHz–0.01 Hz was applied. All measurements were conducted in triplicate. Average values of the module of impedance (0.01 Hz) and its corresponding relative error (logarithmic plot) were determined.

3. Results and discussion

3.1. Effect of current and frequency PEO processing with precursor film

3.1.1. RMS current responses

Fig. 1 shows the effect of applied current density and frequency on the current-time responses during PEO of 6082 alloy with and without precursor film. In all the cases a marked current drop is observed at different times of the

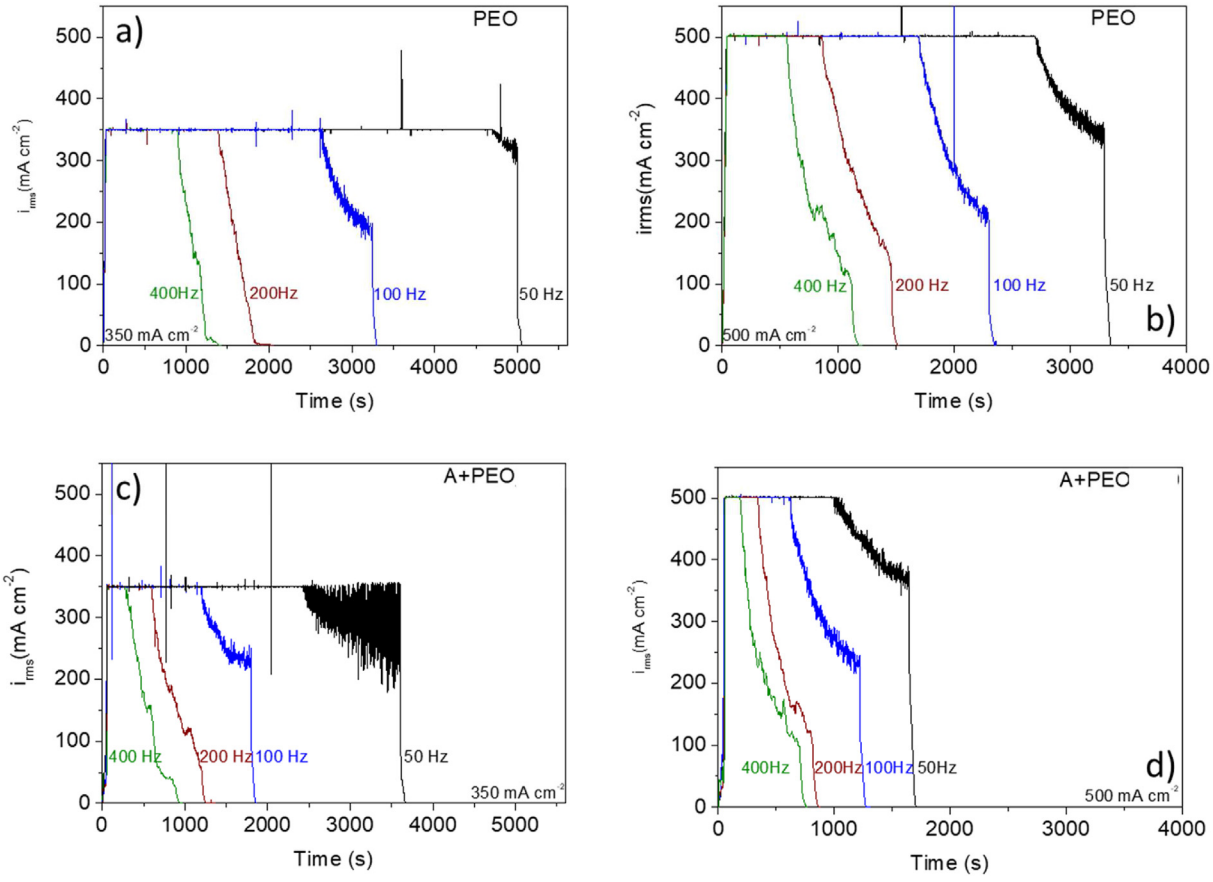

Fig. 1 – Rms current-time responses during PEO of 6082 alloy at different frequencies for: (a) direct PEO, 350 mA cm^{-2}; b) direct PEO, 500 mA cm^{-2}; (c) PEO with precursor film, 350 mA cm^{-2}; (d) PEO with precursor film, 500 mA cm^{-2}.

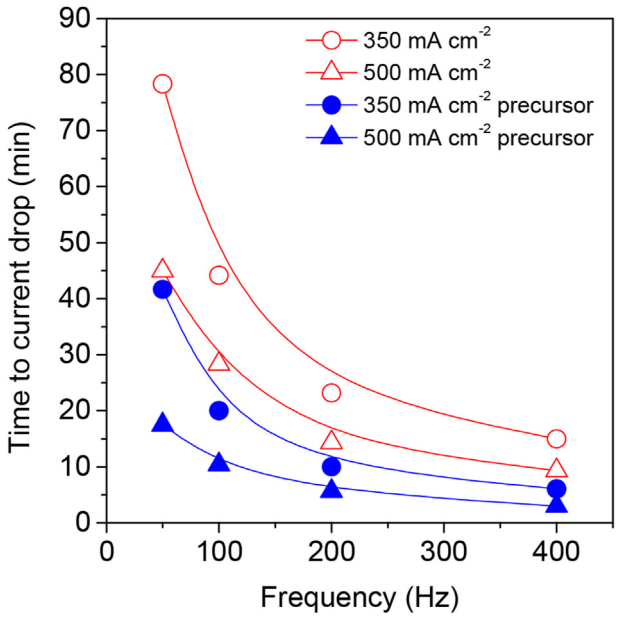

Fig. 2 – Time to current drop vs frequency for the studied systems.

treatment, which is related to the moment when the set input voltage limit is achieved. Theoretically, this limit should be reached at the end of the 60 s ramp. However, initially the impedance of the coating is not high enough for the set voltage, therefore the rms current limit is rapidly reached and maintained. As the coating thickness grows, its impedance increases and the rms voltage value rises accordingly, striving to the set limit. The moment when the voltage limit is reached and the current drop is observed, coincides with the uniform establishment of the "soft sparking" regime over the surface. This is because "soft" type of discharges, typically observed under bipolar and AC conditions with cathodic bias, promote the formation of denser or more compact coatings [15]. The current drop is always expected to occur whenever the voltage-controlled PEO set-up is used and once the impedance of the coating becomes high enough; *i.e.*, the coating growth can proceed with a lower current output.

As shown in Fig. 1 and Fig. 2, the time to current drop (t_{drop}) decreases with increasing frequency (f) and current density and, as expected from previous results, the specimens with precursor anodic film reach the current drop in shorter times [10]. The relationship between t_{drop} and f can be expressed with the following equation (2):

$$\log t_{drop} = K \log f + A \quad (2)$$

where K and A are constants presented in Table 1. Assuming that this relationship is maintained for frequencies beyond the range studied in this work it is feasible to reach a t_{drop} as low as 60 s when using 1500 Hz, 500 mA cm^{-2} and 20 μm-thick precursor film which would be four times less than for a specimen without a precursor. This gives a clear idea of the great potential of precursor films for development of what could be called "flash-PEO" processes.

3.1.2. *Instantaneous current-voltage responses and surface appearance*

Current and voltage waveforms during PEO were recorded at different times for all the specimens. Fig. 3 shows an example of a waveform after 1500 s of PEO at 500 mA cm^{-2} and 50 Hz for a specimen without anodic precursor film. While the voltage waveform reveals a square shape, the anodic current signal features a sharp initial peak up to ~3200 mA cm^{-2} followed by

Table 1 – K and A constants for the relationship between t_{drop} and f (Equation (2)).

	350 mA cm^{-2}			500 mA cm^{-2}		
	K	A	R^2	K	A	R^2
Without precursor	−0.81 ± 0.04	3.26 ± 0.09	0.991	−0.78 ± 0.05	2.98 ± 0.11	0.988
With precursor	−0.94 ± 0.05	3.19 ± 0.12	0.990	−0.85 ± 0.03	2.70 ± 0.06	0.997

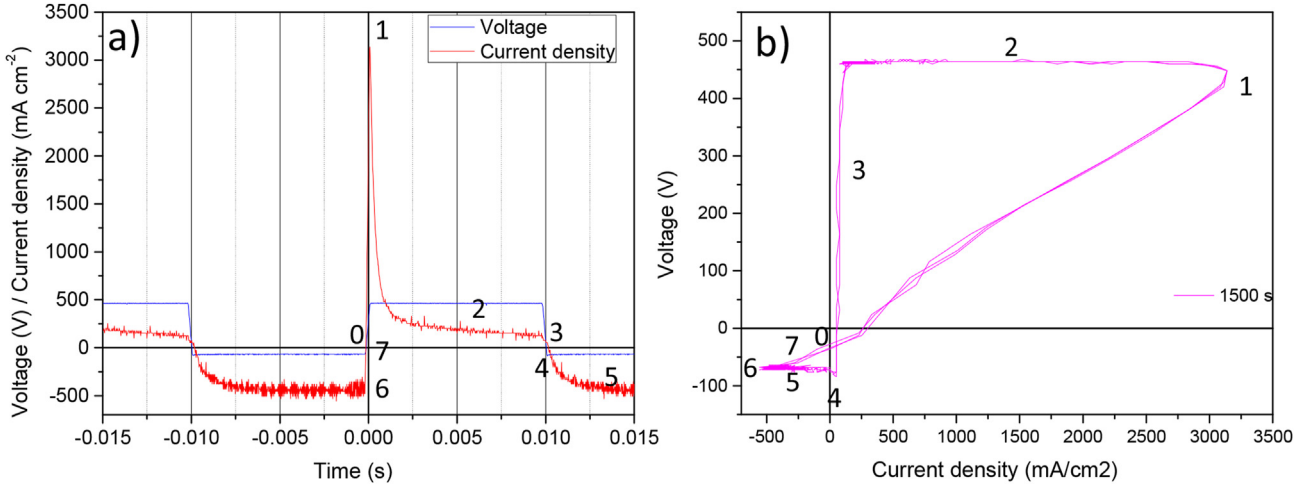

Fig. 3 – Representation of instantaneous voltage and current signals in the form (a) waveform; (b) polarization curve.

an exponential decay down to ~120 mA cm^{-2}. This initial current surge is associated with breakdown and loss of film resistance. The decay is related to regrowth of the oxide film at the locations of microdischarges and the associated increased coating impedance, which eventually leads to extinction of the microdischarges [9]. During the negative pulse, the current density gradually decreases to values around −500 mA cm^{-2}. It is assumed that no microdischarges occur during this period, although in other works [16,17] the presence of cathodic microdischarges has been confirmed at specific conditions during the initial stages of the PEO process of Al and Mg. An alternative representation of instantaneous voltage and current signals in the form of polarization curve is shown in Fig. 3b. The sequence of numbers indicates the correlation between different regions in both plots (Fig. 3).

Fig. 4 shows examples of polarization curves as a function of treatment time with and without precursor. Selected times correspond to different stages during the PEO process; Region I: initial "hard sparking" regime, Region II: combination of "hard" and "soft sparking" and Region III: uniform or homogeneous "soft sparking" regime.

Fig. 4a shows the waveforms obtained for the specimen without precursor film treated at 500 mA cm^{-2} and 50 Hz. At 60 s (Region I), following the direction marked by the arrows, the voltage sharply increases from 0 to ~280 V and the current remains relatively unchanged. This corresponds to thickening of the oxide film similar to what happens during constant current anodizing processes. At ~280 V there is an increase of current, signaling the initiation of microdischarges [18]. Once the maximum voltage is reached (440 V), a sharp drop of

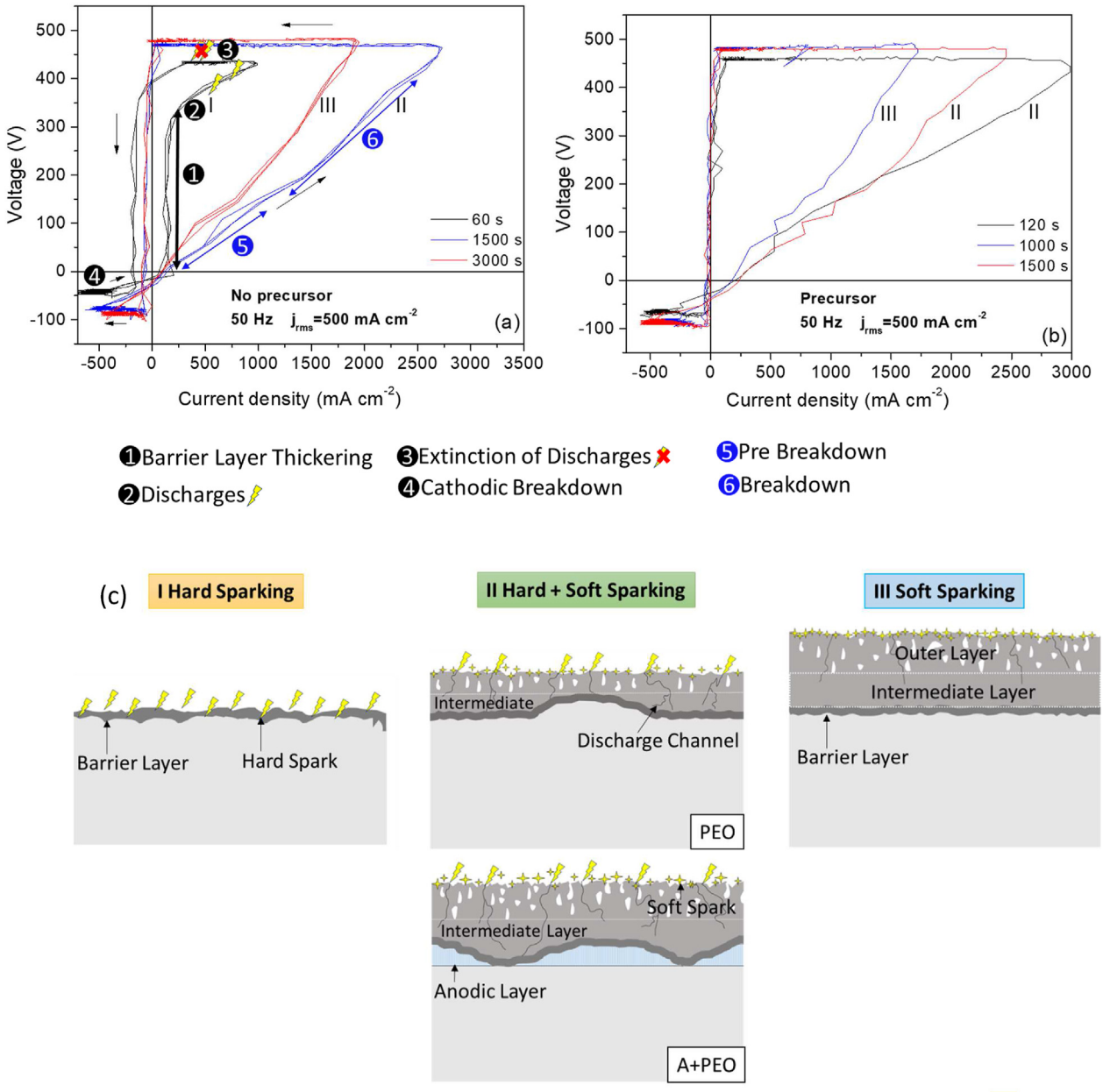

Fig. 4 – Polarization curves as a function of treatment time (a) direct PEO; (b) with precursor. (c) Schematic representation of the stages of coating growth.

current is noted, followed by a voltage drop when the current falls below 300 mA cm^{-2}. This point possibly marks the extinction of microdischarges [18]. When the current reaches zero the voltage of ~400 V is measured which is an indication of an oxide film with a highly capacitive behavior. During the cathodic pulse a sharp increase in cathodic current is noted when a critical negative voltage of ~ −50V is reached. In several works this has been related to the cathodic breakdown of the film during cathodic polarization [18][[17]. Then, the current goes up again linearly and the system still shows the typical response of a capacitor since the voltage is −15 V at zero current. Thickening of the oxide film (1500 s- Region II) shifts the entire polarization curve to higher absolute values of current and both higher positive and negative voltages during the anodic and cathodic pulses, respectively. The lack of a vertical region during the beginning of the positive pulse and the higher current values indicate loss of coating impedance during the pre-breakdown period, possibly associated with heating of the oxide material. Unlike in the 60 s response, the ignition voltage for initiation of microsdischarges cannot be accurately estimated since there is no marked change of slope. Most likely, and as reported by other authors, the ignition voltage increases with the treatment time [18]. High speed camera observations are usually employed in order to determine more accurately the window of existence of the microdischarges [19]. Once the soft sparking has been uniformly established all over the surface (Region III) the ascending anodic slope of the polarization curve shifts to lower currents. This suggests that the loss of coating impedance during the pre-breakdown period associated with heating is overcompensated by the greater impedance of a more uniform and compact coating.

When the precursor is used (Fig. 4b), the most significant change observed in the polarization curves is the absence of Region I, which corresponds to the "hard sparking" regime. From the very early stage of dielectric breakdown the soft sparking regime is established (the higher the frequency and the rms current density the more pronounced is this effect). Then, similarly to the previous case, the polarization curve shifts to lower current values once soft sparking becomes homogeneous. A schematic representation of the stages of coating growth is shown in Fig. 4c.

Fig. 5 shows and example of the development of the surface appearance during the PEO process with precursor film at 500 mA cm^{-2} and 100 Hz. Visual observations during PEO showed that from a very early stage the soft sparking regime is established characterized. It is by a uniform regime of microdischarges that start on the corners and move inward the specimen towards the center until all the coating is homogeneous. After 60 s of treatment the instantaneous population density of microdischarges is ~6.4 microdischarges/cm^2 and the area fraction of coating covering the specimen is ~53%. After 120 s the population density increases to ~95.4 microdischarges/cm^2 with a 92.7% coverage. By 300 s the whole surface of the specimen is completely covered and the coating is now growing homogeneously with ~103.2 microdischarges/cm^2.

3.1.3. *Specific energy consumption, coating thickness and growth rate*

Fig. 6 gathers the specific energy consumption of the PEO process calculated by integration of the instantaneous voltage and current waveforms recorded periodically. The total energy includes the sum of the energy consumed by PEO process and the energy consumed during anodizing process when applicable.

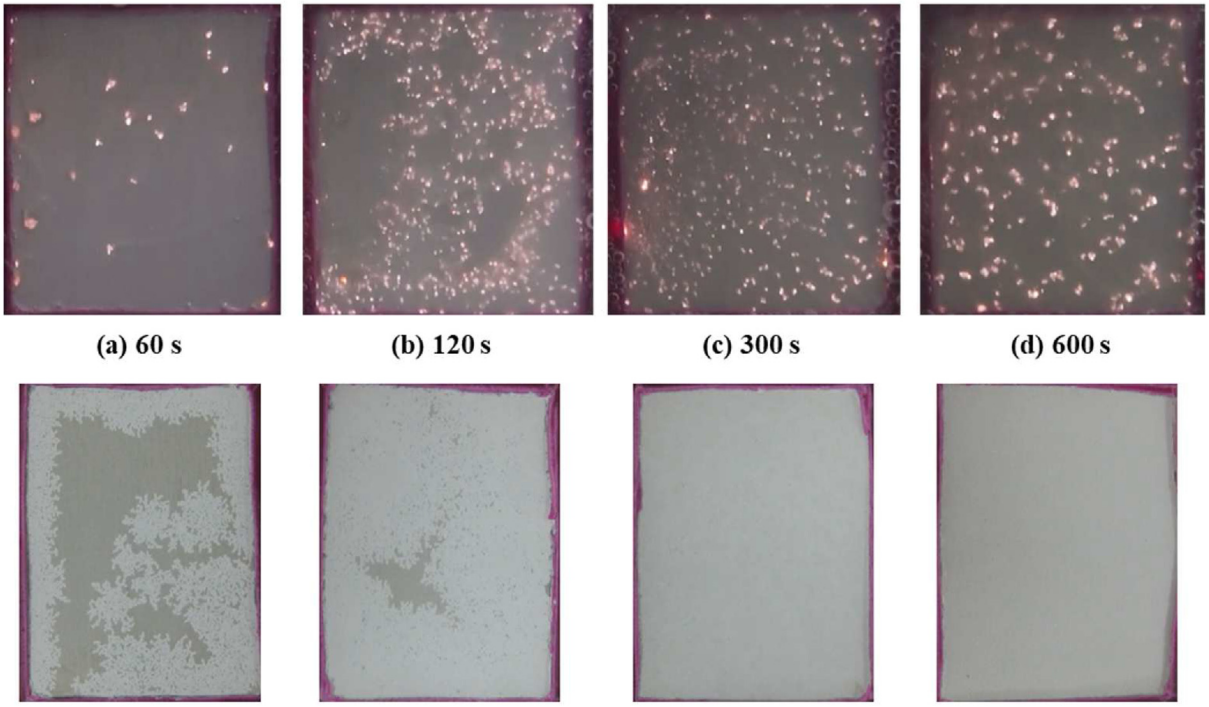

Fig. 5 – Development of the surface appearance during the PEO process with precursor film at 500 mA cm^{-2} and 100 Hz (exposed area 2.5 × 2 cm^2).

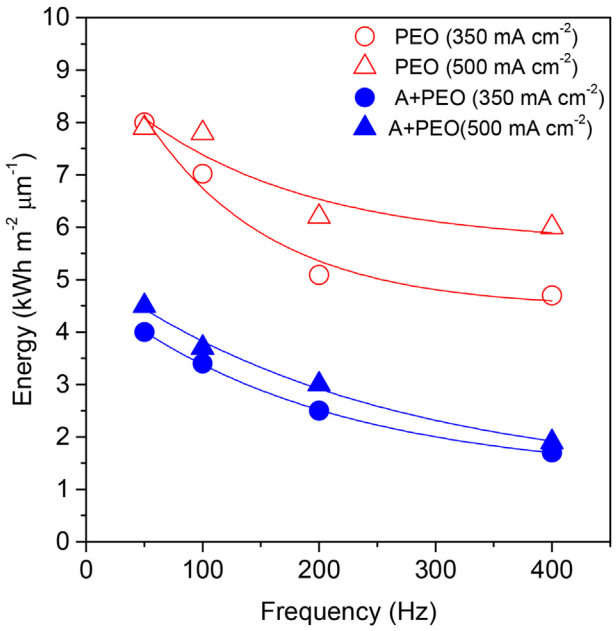

Fig. 6 – Specific energy consumption of the PEO process for the different developed systems.

The comparison of the different treatments in terms of energy savings reveals the following facts.

Regardless of the frequency and current used for the coatings formation, the presence of a precursor anodic film decreases significantly the energy consumption up to 68% in the best case (A + PEO_400 compared to direct PEO_400); which is in concordance with previous studies reporting that the transition to "soft sparking" occurs once a sufficient thickness of the coating has been achieved [8].

Using higher frequencies, a significant reduction in the consumed energy is achieved in all the treated specimens and frequency's influence is more significant in pre-anodized specimens (up to 57% savings for A + PEO_400 compared to A + PEO_50) than in direct PEO (up to 24% savings for PEO_400 compared to PEO_50). The current is the variable that influences the least the overall specific energy consumption. In general, low current density leads to lower energy consumption. In the case of PEO with precursor the savings are in the range of 8–15% depending on the frequency, but a trend cannot be identified. For specimens without the anodic layer there is an increase of the savings for higher frequencies so that for 50 Hz there is no difference on the energy consumed at 350 mA/cm^2 *vs* 500 mA/cm^2, but increasing the frequency, the saving raised up to 20% (for 350 mA/cm^2). It is worth mentioning that a lower current also requires longer treatment times; so, that is a handicap to take into consideration.

The combination of a 20-μm thick precursor anodic porous film, high current (500 mA cm^{-2}) and frequency (400 Hz) during PEO enables up to 76% energy savings compared to direct PEO treatment (50 Hz).

Results found in the present work provide new evidence on the effect of frequency, precursor anodic layer and current density on the energy consumption of PEO coatings. It is stated that both the use of high frequencies and a precursor anodic film highly influence the energy consumption whereas the current applied does not seem to be that significant. Both conditions (high frequency and precursor anodic layer) induce a faster transition into the soft sparking regime as it was visually observed and also determined by the faster drop of the current in the rms curves related to the achievement of the soft sparking mode. The data available for different modes of PEO process of commercial aluminum alloys does not take this variables into consideration and reported values can be as high as 26.7 kW h m^{-2} μm^{-1} [12].

The thickness and average coating growth rate of the PEO coatings determined under different conditions are presented in Table 2. The coating growth rate value is calculated by dividing the final coating thickness by treatment time. The results show that the presence of a precursor anodic film, the use of high frequencies and the application of high current density promote a faster growth rate. A combination of these factors is probably leading to earlier onset of "soft sparking". The longer the material is subjected to "soft sparking", the greater is the overall coating growth rate.

For instance, the highest oxidation kinetics rate (~15.6 μm min^{-1}) is achieved with the combination of the precursor anodic film, the highest frequency (400 Hz) and the highest current density (500 mA cm^{-2}). On the contrary, the lowest growth rate (~1.2 μm min^{-1}) was obtained for the treatment without precursor layer and both the lowest frequency (50 Hz) and current density (350 mA cm^{-2}). These findings are in accordance with the time drop obtained under the different conditions (earlier for specimens with precursor anodic film and higher frequencies and higher current) and are attributed to the faster transition to the soft sparking regime that increases the overall coating growth rate [20,21]. The "soft" nature of the sparks under that regime avoids the undesirable destroying phenomena that occurs during arc regime [20,22].

In general, the available data on the literature does not provide a direct correlation among the different parameters that can be modified during the PEO process (e.g. electrolyte, wave design, voltage, current, frequency) and the final

Table 2 – Parameters of the PEO coatings obtained under the different conditions.

	Thickness (μm)				Growth rate (μm min^{-1})			
	PEO350	A + PEO350	PEO500	A + PEO500	PEO350	A + PEO350	PEO500	A + PEO500
50 Hz	100	97	113	89	1.28	2.1	2.7	5.2
100 Hz	71	68	73	68	1.6	2.8	3.65	4
200 Hz	52	52	62.5	57	2.25	3.63	6.25	10.05
400 Hz	43	40	54	47	2.8	4.2	8.9	15.6

thickness. This fact is due to the interaction of the different factors during the development of the coating that change the discharge thermodynamics and the characteristics of the obtained layer. In the particular case of the applied current, it has been reported that the coating thickness increase with increase current density for DC PEO coatings [23,24]. With regards the effect of frequency, results obtained in the present work differ from the ones reported by Martin et al. [21] who showed that increasing the anodic current density and the pulse frequency simultaneously results in thicker and more compact coatings, which was related to an increased density of micro-discharges that promotes the early transition to the "soft sparking" mode. Possibly the different behavior observed is associated with the different treatment times, while Martin used a fixed treatment time, in this work the treatment was stopped 600 s after the current drop was observed or when the rms current value decreased to values below 100 mA cm^{-2} which in the present work led to thinner coatings, despite having a greater growth rate.

Findings reveal that among the different electrical parameters, the current applied influences the least the final energy consumed and growth rate in comparison with the more significant effect of frequency and precursor film. Based on that, specimens developed under the extreme conditions (50 Hz and 400 Hz) with and without precursor anodic film were selected for further detailed studies. The selected current was 500 mA cm^{-2} due to the obtained faster growth rate along with no significant differences on the energy consumed compared to 350 mA cm^{-2}.

Table 3 – Surface roughness.

	Sa (μm)	Sz (μm)	$HV_{0.05}$
PEO_50	5.6 ± 0.7	48 ± 4	916 ± 48
A + PEO_50	5.7 ± 0.4	44 ± 1	643 ± 29
PEO_400	4.5 ± 0.5	39 ± 3	764 ± 47
A + PEO_400	5.1 ± 0.2	43 ± 3	447 ± 46

3.2. *Coatings characterization*

SEM surface views of selected coated specimens are shown in Fig. 7. All the layers reveal the typical surface morphology of plasma electrolytic oxidation coatings with a mixture of pancake-like structure surrounded by a sponge-like morphology [25]. The micro-cracks and pores are located at the sites of the discharge channels and associated with thermal stresses and gas evolution through the molten oxide material during the PEO treatment [26].

The presence of the precursor anodic layer does not affect significantly the final surface morphology of the coatings. It can be observed that the use of a high frequency leads to the formation of a more sponge-like structure covering basically the whole surface. The pancake-like surface morphology has been associated with the exposition to hard sparking with the characteristic discharge channel usually localized at the centre of the pancake; whereas an sponge-like structure has been related to a softer sparking regime [27]. The surface roughness values of the coatings (Table 3) are quite similar

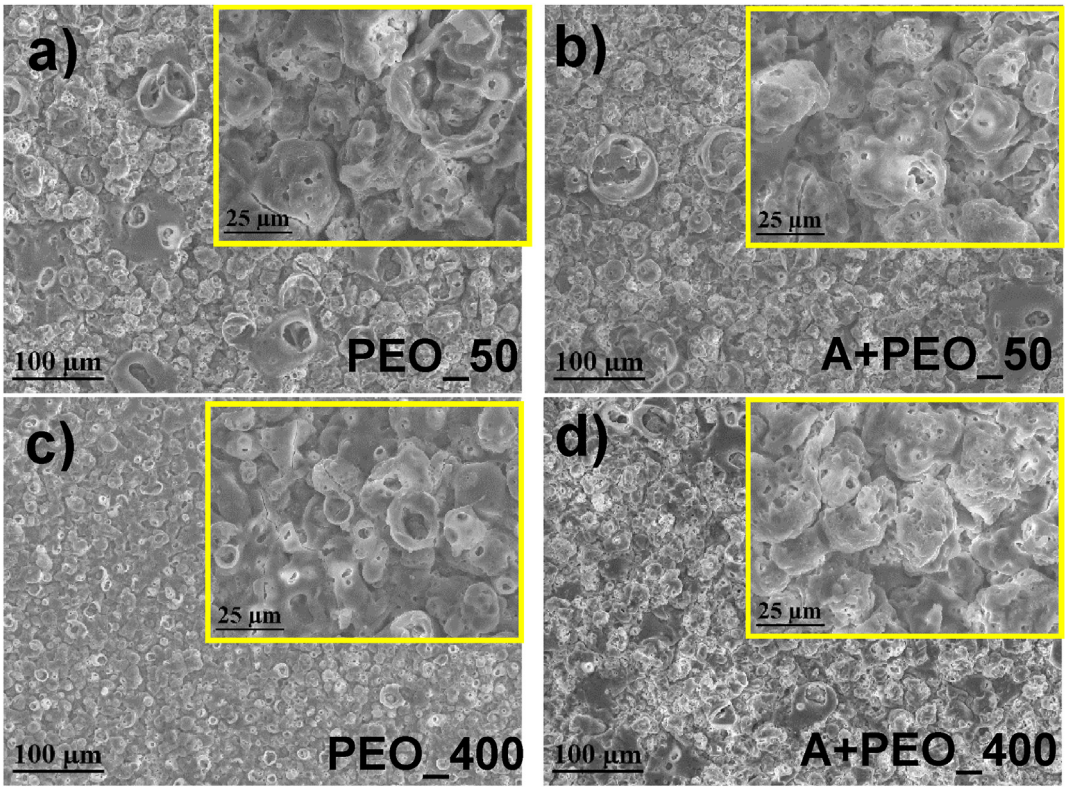

Fig. 7 – SEM surface views of selected coatings (a) direct PEO, 50 Hz; (b) PEO with precursor, 50 Hz; (c) direct PEO, 400 Hz; (d) PEO with precursor, 400 Hz.

and only a slight decrease is observed when the frequency increases, which can be associated with more areas of sponge-like morphology.

The cross sections of the studied coatings (Fig. 8) show a thickness in a range of (~40–100) μm depending on the treatment. The presence of three distinct sublayers (indicated in Fig. 8 b) is observed which are characteristic of PEO coatings growth on aluminium alloys: highly-porous outer part, denser intermediate layer with smaller porosity and a sub-micron size barrier layer [28]. The pre-anodized alloys reveal a

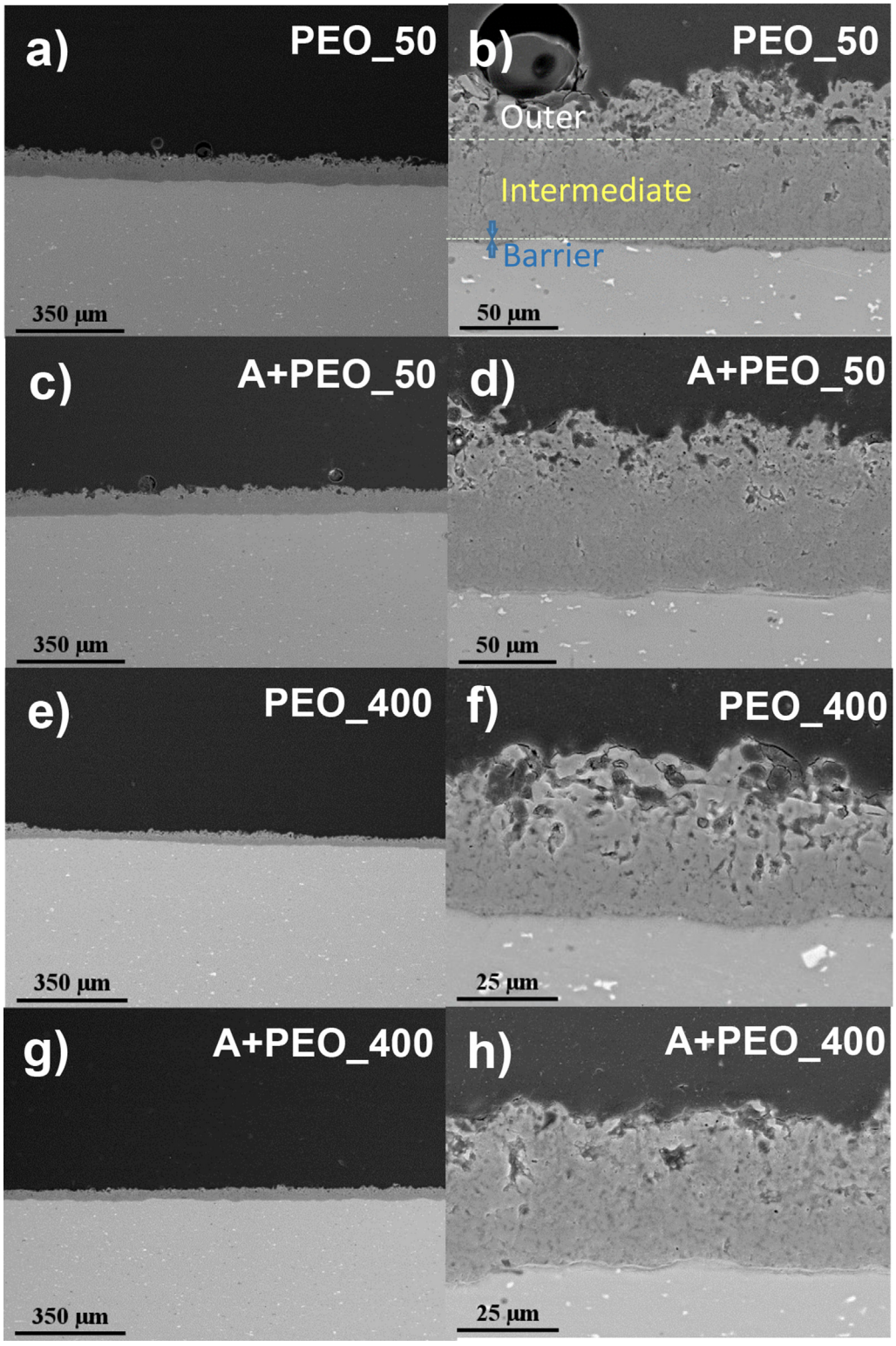

Fig. 8 – Backscattered electron images of the PEO coating cross-sections: (a,b) direct PEO, 50 Hz; (c,d) PEO with precursor, 50 Hz; (e,f) direct PEO, 400 Hz; (g,h) PEO with precursor, 400 Hz.

growth rate 2 or 3 times higher than non-anodized PEO for treatments conducted at 50 Hz and 400 Hz respectively. Therefore, the anodic precursor film promotes even a faster growth rate for treatments conducted at higher frequencies (Table 3).

It is worth mentioning that layers developed after pre-anodizing seem to be slightly denser. However, PEO coatings tend to contain inter-connected networks of fine-scale porosity not detectable by conventional microscopy techniques [29]. Rogov [30] analysed by high-angle annular dark-field imaging (HAADF) the microstructural features of PEO coatings developed under arc and "soft-sparking" conditions at the metal/oxide interface and observed significant differences. Under the arc condition, the first few microns from the interface showed a combination of nano- (50–100 nm) and micro-sized (1 μm) porosity, while the coatings formed under "soft sparking" condition showed a thin sub-layer with low nano-porosity, a 3–4 μm sponge-like band with nano-sized porosity, followed by a more compact region.

XRD patters of all coatings (Fig. 9) reveal peaks corresponding to Al (ICDD card 00-004-0787), indicating that the X-Ray beam reached the substrate although the diffraction set-up was designed to have an approximate penetration of the X-rays below 5 μm (for alumina density values of 4.05 g/cm^3 - crystalline and 2.66–3.4 g/cm^3 - amorphous). The identification of the substrate may be associated with the inherent porosity of the coatings and/or some edge effect (e.g. coating damage after cutting the coated sample).

Regarding the crystalline phases of the coatings, the applied frequency seems to have an important effect on the different formed phases, whereas no substantial differences between samples with and without precursor anodic layers are observed.

Coatings developed under low frequencies (50 Hz) are composed of a mixture of alumina γ-Al_2O_3 (ICDD card 00-050-0741), α-Al_2O_3 (ICDD card 00-046-1212) phase and mullite (ICDD card 01-079-1450). The formation of high-temperature phases such as α-Al_2O_3 and mullite are associated with mainly two factors: i) a high temperature of non-equilibrium micro-discharges that develop over the processed surface [31] and ii) a longer duration of the treatment (due to the delay in current drop for the layers at 50 Hz). The fact that specimens were exposed to the microdischarges and high temperatures for longer time, which contributed to formation of hard alumina phases [26], is in concordance with other studies reporting that long PEO treatments lead to the formation of more high-temperature stable phases [32].

For coatings developed a high frequencies, the major constituent formed is γ-Al_2O_3, which is associated with high cooling rates favoring the solidification of molten alumina into metastable γ-Al_2O_3 nuclei over the stable α-Al_2O_3 phase [33].

The fact that PEO coatings with high growth rate produce low temperature crystaline phases was reported for oxide layers developed in electrolytes with high silicate concentrations [34]. This is in accordance with the results obtained in this work in which low temperature crystalline phases were obtained in PEO coatings with high growth rate (developed at 400 Hz).

It is clear that high-temperature stable phases (α-Al_2O_3 and mullite) are only found in coatings formed at 50 Hz (with a lower growth rate compared to layers developed at 400 Hz). It is also worthy to mention that among those coatings (PEO_50 Hz and A + PEO-50 Hz) the crystalline phases peaks are more intense in precursor-free coating formed in longest treatment time and with the lowest growth rate.

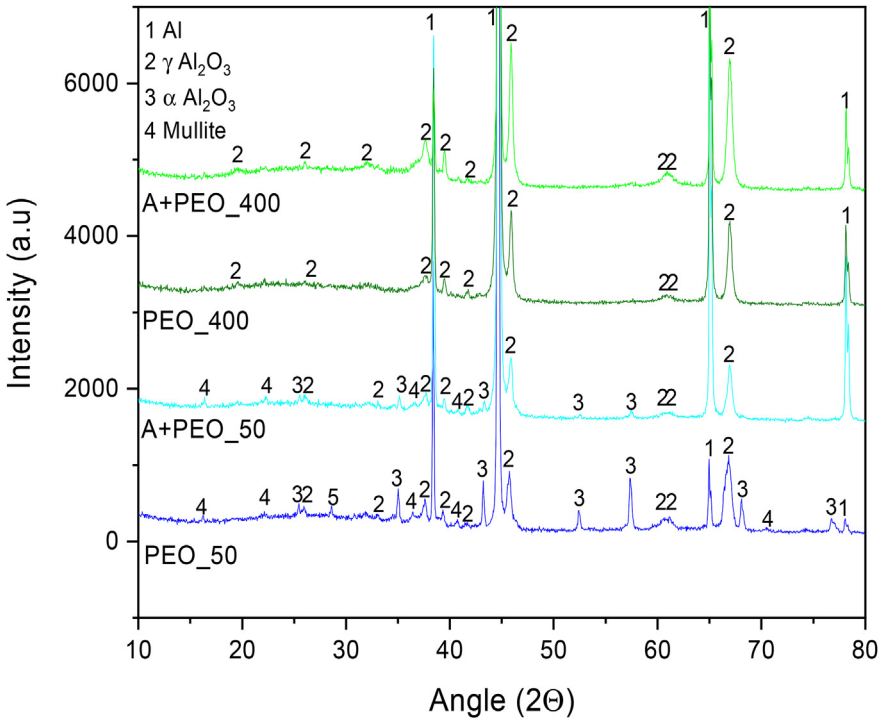

Fig. 9 – X-ray diffraction patterns of selected coatings.

Table 3 shows the microhardness values ($HV_{0.05}$) of the developed coatings. As expected, the coating with a higher amount of α-Al_2O_3 (PEO_50) shows the highest value of hardness (916 ± 48 $HV_{0.05}$), while the one with a higher proportion of γ-Al_2O_3 (A + PEO_400) presents the lowest value (447 ± 46 $HV_{0.05}$). Interestingly, the PEO_400 shows a higher hardness (764 ± 47 $HV_{0.05}$) than A + PEO_50 (643 ± 29 $HV_{0.05}$) despite having a slightly smaller amount of α-Al_2O_3. This could be associated with two factors, (i) the presence of mullite, which is slightly softer than γ-Al_2O_3 (14 *vs.* 17 GPa [35]) and (ii) the microstructural changes induced by the precursor anodic film that promotes the formation of inter-connected networks of fine-scale porosity that might affect the overall hardness of the material.

3.3. *Wear properties*

Findings in the present work reveal that the appropriate selection of the frequency and a pre-anodizing step lead to a considerable reduction in energy consumption. However, it is essential to ensure that both wear and corrosion performance of the oxide layer are not compromised.

The average values of friction coefficients were in the range of (0.75–0.83) with non-significant differences among the developed coatings. The obtained results were relatively high and comparable to those found in other works [33,36].

Fig. 10 shows the wear volume and the calculated wear rate of the selected PEO coatings. The presented results are the average of 3 specimens from which 20 μm of the coating was removed to avoid the contribution of the looser outer part of the coating. These results demonstrate the benefit of using high frequency (400 Hz) PEO treatments for enhanced wear performance with respect to the coatings formed at 50 Hz. The wear rate values are reduced up to one order of magnitude from 4.234×10^{-5} for PEO_50 to 4.752×10^{-6} $mm^3\ N^{-1}\ m^{-1}$ for PEO_400, despite its lower microhardness. This is probably related to the change in the crystallinity of the main forming phases and the modification of the porosity of the intermediate layer of the coating. It has been stated repeatedly that the early establishment of the "soft-spark" regime leads to a densification of the intermediate layer which contributes positively to the wear response.

Regarding the use of the precursor anodic film, a different trend was found depending on the frequency range. In the case of 50 Hz, the precursor anodic film shows a positive effect with a reduction of the wear rate up to 57% for the pre-anodized specimen. Whereas in the case of 400 Hz, the specimen with the anodic precursor film (A + PEO_400) reveals a slightly worse wear performance, although it is still 18% better than A + PEO_50 and 65% better than PEO_50. This improvement in the wear rate of the coating that also presents the highest energy efficiency (76% energy saving for A + PEO_400 *vs.* PEO_50) is still 12% better than the wear rate of hard chrome plating coatings tested under a similar load (1.7×10^{-5} $mm^3\ N^{-1}\ m^{-1}$) [33], which are known for their exceptional tribological properties.

The backscattered SEM images of the wear tracks of all PEO specimens are shown in Fig. 11a–d. The differences between coatings in the wear track width are evident and are in good agreement with the Wr trend shown in the previous section: PEO_50 < A + PEO_50 < A + PEO_400 < PEO_400. The higher magnification details of the wear track of the coatings developed at 50 Hz (Fig. 11e–f) show a relatively uniform and cracked tribolayer. The track of the coatings developed at 400 Hz show some slight differences (Fig. 11 g-h). PEO_400 shows regions with a high density of microcraks surrounded by uniform monolithic regions containing fewer but bigger cracks, probably formed as a consequence of the stresses induced by the sliding counterpart [37]. In the latter region, some abrasion grooves parallel to the sliding direction can also be identified. The A + PEO_400 shows a rougher surface and some signs of delamination, which are commonly observed in PEO coatings [33]. The cross sectional micrographs of all coatings do not show a noticeable curvature of the surface and in all cases the worn tracks show a relatively uniform tribolayer across the whole tested area.

Table 4 gathers the EDS measurements located in the wear track (point 1 marked in Fig. 11 i-j). It discloses the presence of elements from the oxidation of the substrate (O, Al) and species derived from electrolyte (Na, Si, P, K). The treatments parameters and the removal of the looser outer part of the coating might influence in the obtained composition. It is worth mentioning that the analysis also shows relatively high amounts of W (12 at. %) for the PEO_50 layer, indicating the damage of the WC counterpart and its transfer to the tribolayer (adhesion during the friction process). The amount of W is lower for the rest of the coatings (down to 0.6 at.% for PEO_400) which is in agreement with the values of wear volumes obtained and SEM observations.

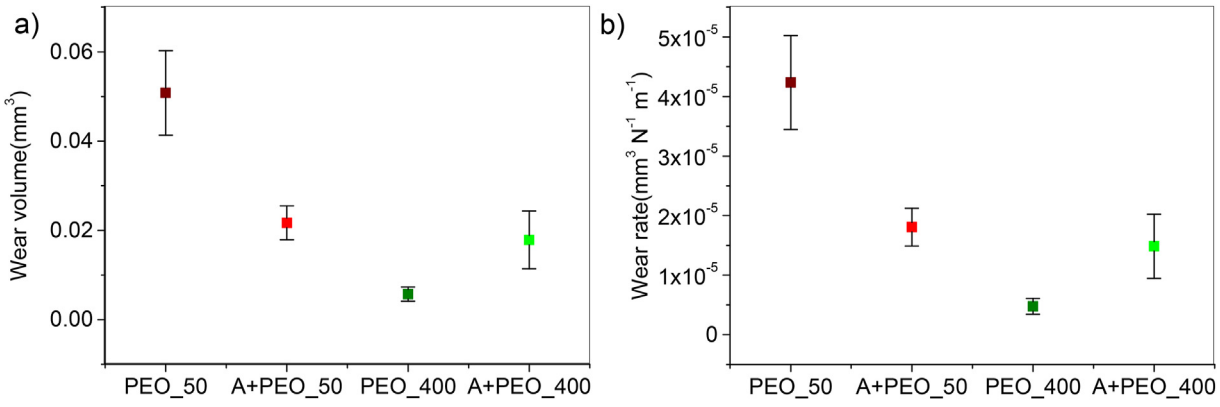

Fig. 10 – (a) Wear volume and (b) estimated wear rate for the selected coatings.

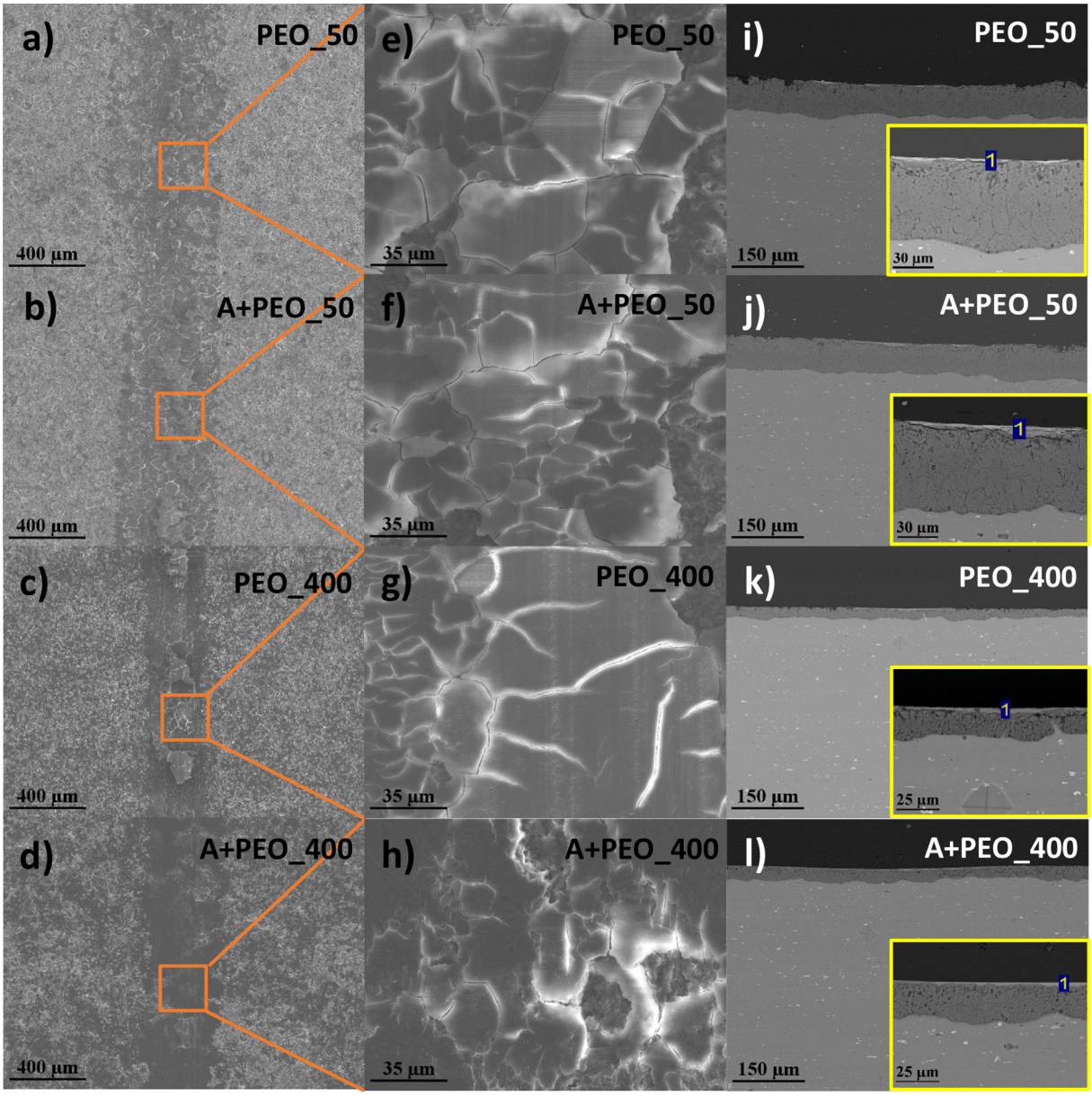

Fig. 11 – SEM images of the wear tracks of selected PEO specimens: (a–d) plan view; (e–h) detailed inside the track; (i–l) BSE cross-section. (a,e,i) direct PEO, 50 Hz; (b,f,j) PEO with precursor, 50 Hz; (c,g,k) direct PEO, 400 Hz; (d,h,l) PEO with precursor, 400 Hz.

3.4. *Corrosion behaviour*

Electrochemical Impedance Spectroscopy (EIS) was used to evaluate the corrosion resistance in naturally aerated NaCl 3.5 wt% solution after 1 h of immersion. Bode plots are depicted in supplementary material (Supplementary Fig. S1).

Table 4 – Composition determined by point EDS analyses for Fig. 11(i–l) (at. %).

	O	Al	Na	Si	P	K	W
PEO_50	61.3	17.1	0.4	0.3	0.6	1.2	12.1
A + PEO_50	75.9	15.9	0.3	0.2	0.3	0.7	1.4
PEO_400	82.5	13.7	–	0.5	0.3	0.2	0.6
A + PEO_400	80.5	15.9	–	0.7	0.3	4.2	1.3

Coatings developed at 400 Hz clearly show two capacitive relaxation processes at high and low frequencies related to the responses of the porous part (combination of outer and intermediate layers) and inner barrier layer. For coatings formed under 50 Hz the high-frequency relaxation process is hard to distinguish, which can be associated with a weaker response of the porous part probably due to the presence of more through-going discharge channels and porosity. The precursor anodic film does not seem to have a significant influence on the magnitude or phase of the transfer function versus frequency.

Fig. 12 shows the module of the impedance at low frequencies, which provides a good estimation of the overall corrosion performance of the material, and its relative error. Increasing the processing frequency results in an

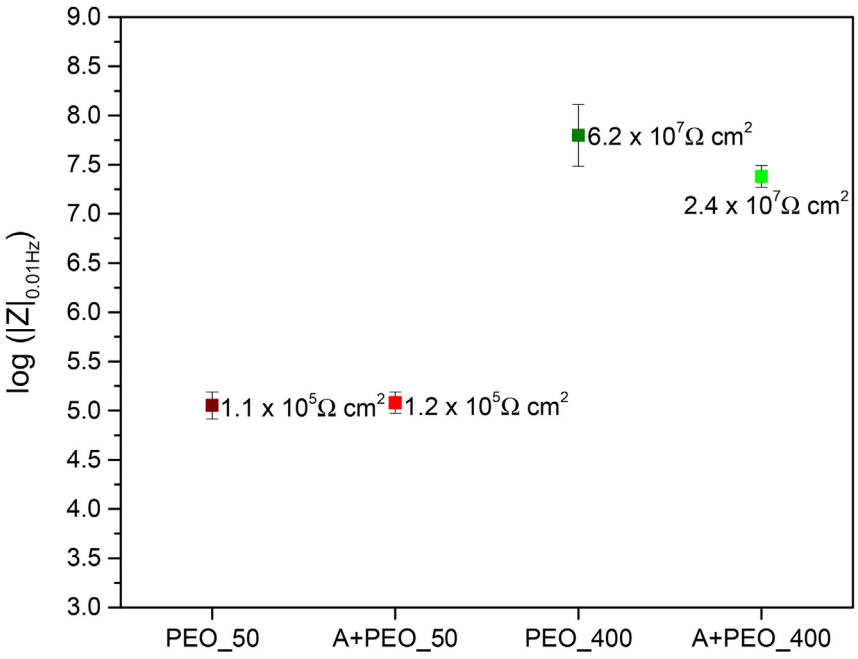

Fig. 12 – Module of the impedance at 0.01 Hz (log scale) along with its relative error after 1 h of immersion in naturally aerated NaCl 3.5 wt% solution. The values of |Z| are given in Ω cm^2.

improvement of 2–3 orders of magnitude of the overall corrosion resistance of the coatings, while the presence of the precursor anodic film does not influence significantly the corrosion response. The positive effect of high processing frequencies has been reported previously for both Al [14] and Mg [38] based materials. Such improvement is usually associated to the refined microstructure resulted from the change of the thermodynamic properties of the microdischarges; high frequencies lead to shorter pulse times, which promotes the formation of a higher population density of less intense microdischarges. This results in a refined microstructure with reduced porosity in terms of pore size, which impedes the access of the electrolyte and therefore, delaying the corrosion initiation process. Moreover, the reduction of the intensity of the microdischarges also prevents the damage of the inner compact barrier layer during the arc regime [39].

As discussed in Section 3.1, both increasing the processing frequency and the application of the precursor anodic layer, promote the transition from the arc to the "soft-sparking" regime with the consequent microstructural improvement. Additionally, the presence of the precursor anodic layer promotes a faster transition. All coatings have been exposed to the "soft sparking" regime for the same period of time (600 s), while the exposure to the arc conditions is different in each coating since the transition to the "soft" regime depends on the used processing conditions. Therefore, the coatings with the precursor anodic layer were processed for a lower treatment time compared to their counterparts. While the coatings developed under "soft sparking" are usually denser and more homogeneous which leads to a higher corrosion resistance, increasing the treatment time does not have a straightforward influence on the properties of the coating: longer treatment times under arc conditions increases the porosity, however it also leads to thicker coatings [40]. As the film grows thicker, the size of the discharge channels increases because a higher energies are needed for the current to pass through the film [41]. Therefore, it is key to optimize the treatment time to minimize the porosity while maintaining a sufficient thickness to maximize the corrosion properties of the coatings. The results presented in Fig. 12 clearly show the previously described trends. The coatings developed at 400 Hz had shorter processing times (~1200 and ~750 s for PEO_400 and A + PEO_400, respectively) than those obtained at 50 Hz (~3350 and ~1700 s for PEO_50 and A + PEO_50, respectively) (Fig. 1), limiting the negative effect of the arc stage on the porosity. However, when comparing the performance of PEO_400 and A + PEO_400 it can be observed that the reduction of the processing time as a consequence of the precursor anodic layer, slightly decreases the corrosion resistance. This is probably related to the slightly lower thickness of the coating.

It can be concluded that the modification of the frequency has a stronger influence on the corrosion response than the presence of the anodic precursor. The best corrosion response was obtained for PEO_400 followed closely by A + PEO_400 indicating that the proposed strategy, not only improves the energy efficiency of the process, but also increases the corrosion performance of the material.

4. Conclusions

In this work three strategies are evaluated to improve the energy efficiency of PEO processes on aluminium substrates: optimization of the processing frequency, processing current density and application of a precursor anodic film. The main conclusions are summarised as follows:

- The time to current drop decreases with increasing frequency and current density and the specimens with precursor anodic film reach the current drop in shorter times.
- Both the use of high frequencies and a precursor anodic film highly influence the energy consumption whereas the applied current does not seem to be that significant.
- The combination of a 20-μm thick precursor anodic porous film and high current (500 mA cm^{-2}) and frequency (400 Hz) during PEO enables up to 76% energy savings compared to direct PEO treatment.
- The improvement on the wear and corrosion performance is related to the microstructural refinement associated with high frequency processing and early transaction to the "soft-sparking regime".
- The modification of the frequency has a stronger influence on the corrosion response than the presence of the anodic precursor. PEO_400 is the coating with the best corrosion and wear performance and shows an improvement in the energy savings of 24% compared to direct PEO at 50 Hz.
- A + PEO_400 Hz is the coating with the highest energy savings of 76% and it maintains very similar wear and corrosion properties to those of PEO_400.

Declaration of Competing Interest

The authors declare that they have no known competing financial interests or personal relationships that could have appeared to influence the work reported in this paper.

Acknowledgements

The authors gratefully acknowledge the support of PID2021-124341OB-C22 (MCIU/AEI/FEDER, UE) and ADITIMAT-CM (S2018/NMT-4411, Regional Government of Madrid and EUStructural Funds). M. Mohedano is grateful for the support of RYC-2017-21843 Ministerio de Ciencia e Innovación. B. Mingo is supported by the Royal Academy of Engineering through the RAEng Research Fellowship and by EPSRC (EP /V026097/1).

Appendix A. Supplementary data

Supplementary data to this article can be found online at https://doi.org/10.1016/j.jmrt.2022.10.049.

REFERENCES

[1] Snizhko L, Yerokhin A, Gurevina N, Patalakha V, Matthews A. Excessive oxygen evolution during plasma electrolytic oxidation of aluminium. Thin Solid Films 2007;516:460–4.
[2] del Olmo R, Mohedano M, Visser P, Matykina E, Arrabal R. Flash-PEO coatings loaded with corrosion inhibitors on AA2024. Surf Coating Technol 2020;402:126317.
[3] Dehnavi V, Luan BL, Shoesmith DW, Liu XY, Rohani S. Effect of duty cycle and applied current frequency on plasma electrolytic oxidation (PEO) coating growth behavior. Surf Coating Technol 2013;226:100–7.
[4] Wei C, Tian X, Yang S, Wang X, Fu RK, Chu PK. Anode current effects in plasma electrolytic oxidation. Surf Coating Technol 2007;201:5021–4.
[5] Matykina E, Arrabal R, Skeldon P, Thompson G. Optimisation of the plasma electrolytic oxidation process efficiency on aluminium. Surf Interface Anal: An International Journal devoted to the development and application of techniques for the analysis of surfaces, interfaces and thin films 2010;42:221–6.
[6] H-x Li, R-g Song. Ji Z-g. Effects of nano-additive TiO2 on performance of micro-arc oxidation coatings formed on 6063 aluminum alloy. Trans Nonferrous Metals Soc China 2013;23:406–11.
[7] Matykina E, Arrabal R, Mohamed A, Skeldon P, Thompson GE. Plasma electrolytic oxidation of pre-anodized aluminium. Corrosion Sci 2009;51:2897–905.
[8] Matykina E, Arrabal R, Skeldon P, Thompson G, Belenguer P. AC PEO of aluminium with porous alumina precursor films. Surf Coating Technol 2010;205:1668–78.
[9] Matykina E, Arrabal R, Pardo A, Mohedano M, Mingo B, Rodríguez I, et al. Energy-efficient PEO process of aluminium alloys. Mater Lett 2014;127:13–6.
[10] Mohedano M, Mingo B, Mora-Sánchez H, Matykina E, Arrabal R. Effects of pre-anodizing and phosphates on energy consumption and corrosion performance of PEO coatings on AA6082. Surf Coating Technol 2021;409:126892.
[11] Clyne TW, Troughton SC. A review of recent work on discharge characteristics during plasma electrolytic oxidation of various metals. Int Mater Rev 2019;64:127–62.
[12] Yerokhin AL, Shatrov A, Samsonov V, Shashkov P, Pilkington A, Leyland A, et al. Oxide ceramic coatings on aluminium alloys produced by a pulsed bipolar plasma electrolytic oxidation process. Surf Coating Technol 2005;199:150–7.
[13] An L-y, Ma Y, Yan X-x, Wang S, Wang Z-y. Effects of electrical parameters and their interactions on plasma electrolytic oxidation coatings on aluminum substrates. Trans Nonferrous Metals Soc China 2020;30:883–95.
[14] Asgari M, Rouhaghdam AS, Daneshmaslak A. Effect of pulsed current frequency on morphology and corrosion behavior of plasma electrolytic oxidation on aluminum. Protect Met Phys Chem Surface 2020;56:575–83.
[15] Rogov AB, Yerokhin A, Matthews A. The role of cathodic current in plasma electrolytic oxidation of aluminum: phenomenological concepts of the "soft sparking" mode. Langmuir 2017;33:11059–69.
[16] Nomine A, Martin J, Henrion G, Belmonte T. Effect of cathodic micro-discharges on oxide growth during plasma electrolytic oxidation (PEO). Surf Coating Technol 2015;269:131–7.
[17] Sah SP, Tsuji E, Aoki Y, Habazaki H. Cathodic pulse breakdown of anodic films on aluminium in alkaline silicate electrolyte – understanding the role of cathodic half-cycle in AC plasma electrolytic oxidation. Corrosion Sci 2012;55:90–6.
[18] Suminov I, Belkin P, Apelfeld A, Lyudin V, Krit B, Borisov A. Plasma electrolytic surface modification of metals and alloys, Monography, in, Moscow: Tekhnosfera. 2011.
[19] Troughton SC, Clyne TW. Cathodic discharges during high frequency plasma electrolytic oxidation. Surf Coating Technol 2018;352:591–9.
[20] Jaspard-Mécuson F, Czerwiec T, Henrion G, Belmonte T, Dujardin L, Viola A, et al. Tailored aluminium oxide layers by bipolar current adjustment in the Plasma Electrolytic

Oxidation (PEO) process. Surf Coating Technol 2007;201:8677–82.
[21] Martin J, Melhem A, Shchedrina I, Duchanoy T, Nominé A, Henrion G, et al. Effects of electrical parameters on plasma electrolytic oxidation of aluminium. Surf Coating Technol 2013;221:70–6.
[22] Sundararajan G, Rama Krishna L. Mechanisms underlying the formation of thick alumina coatings through the MAO coating technology. Surf Coating Technol 2003;167:269–77.
[23] Xiang N, Song R-g, Zhuang J-j, Song R-x, Lu X-y, Su X-p. Effects of current density on microstructure and properties of plasma electrolytic oxidation ceramic coatings formed on 6063 aluminum alloy. Trans Nonferrous Metals Soc China 2016;26:806–13.
[24] Khan RHU, Yerokhin A, Li X, Dong H, Matthews A. Surface characterisation of DC plasma electrolytic oxidation treated 6082 aluminium alloy: effect of current density and electrolyte concentration. Surf Coating Technol 2010;205:1679–88.
[25] Matykina E, Arrabal R, Skeldon P, Thompson GE. Investigation of the growth processes of coatings formed by AC plasma electrolytic oxidation of aluminium. Electrochim Acta 2009;54:6767–78.
[26] Yerokhin AL, Nie X, Leyland A, Matthews A, Dowey SJ. Plasma electrolysis for surface engineering. Surf Coating Technol 1999;122:73–93.
[27] Martin J, Nominé A, Brochard F, Briançon JL, Noël C, Belmonte T, et al. Delay in micro-discharges appearance during PEO of Al: evidence of a mechanism of charge accumulation at the electrolyte/oxide interface. Appl Surf Sci 2017;410:29–41.
[28] Matykina E, Arrabal R, Mohedano M, Mingo B, Gonzalez J, Pardo A, et al. Recent advances in energy efficient PEO processing of aluminium alloys. Trans Nonferrous Metals Soc China 2017;27:1439–54.
[29] Curran JA, Kalkancı H, Magurova Y, Clyne TW. Mullite-rich plasma electrolytic oxide coatings for thermal barrier applications. Surf Coating Technol 2007;201:8683–7.
[30] Rogov AB, Nemcova A, Hashimoto T, Matthews A, Yerokhin A. Analysis of electrical response, gas evolution and coating morphology during transition to soft sparking PEO of Al. Surface and Coatings Technology 2022:128142.
[31] Martin J, Nominé A, Ntomprougkidis V, Migot S, Bruyère S, Soldera F, et al. Formation of a metastable nanostructured mullite during Plasma Electrolytic Oxidation of aluminium in "soft" regime condition. Mater Des 2019;180:107977.
[32] Agureev L, Savushkina S, Ashmarin A, Borisov A, Apelfeld A, Anikin K, et al. Study of plasma electrolytic oxidation coatings on aluminum composites. Metals 2018;8:459.
[33] Arrabal R, Mohedano M, Matykina E, Pardo A, Mingo B, Merino MC. Characterization and wear behaviour of PEO coatings on 6082-T6 aluminium alloy with incorporated α-Al2O3 particles. Surf Coating Technol 2015;269:64–73.
[34] Pillai AM, Ghosh R, Dey A, Prajwal K, Rajendra A, Sharma AK, et al. Crystalline and amorphous PEO based ceramic coatings on AA6061: nanoindentation and corrosion studies. Ceram Int 2021;47:14707–16.
[35] Costa TM, Gallas MR, Benvenutti EV, da Jornada JA. Study of nanocrystalline γ-Al2O3 produced by high-pressure compaction. J Phys Chem B 1999;103:4278–84.
[36] Terleeva OP, Slonova AI, Rogov AB, Matthews A, Yerokhin A. Wear resistant coatings with a high friction coefficient produced by plasma electrolytic oxidation of Al alloys in electrolytes with basalt mineral powder additions. Materials 2019;12:2738.
[37] Mora-Sanchez H, del Olmo R, Rams J, Torres B, Mohedano M, Matykina E, et al. Hard anodizing and plasma electrolytic oxidation of an additively manufactured Al-Si alloy. Surf Coating Technol 2021;420:127339.
[38] Mingo B, Guo Y, Němcová A, Gholinia A, Mohedano M, Sun M, et al. Incorporation of halloysite nanotubes into forsterite surface layer during plasma electrolytic oxidation of AM50 Mg alloy. Electrochim Acta 2019;299:772–88.
[39] Zhang X, Zhang Y, Chang L, Jiang Z, Yao Z, Liu X. Effects of frequency on growth process of plasma electrolytic oxidation coating. Mater Chem Phys 2012;132:909–15.
[40] MDM Tavares, JDO Vitoriano, RCLD Silva, Franco AR, GBD Souza, JAPD Costa, et al. Effect of duty cycle and treatment time on electrolytic plasma oxidation of commercially pure Al samples. J Mater Res Technol 2019;8:2141–7.
[41] Dehnavi V, Shoesmith DW, Luan BL, Yari M, Liu XY, Rohani S. Corrosion properties of plasma electrolytic oxidation coatings on an aluminium alloy—The effect of the PEO process stage. Mater Chem Phys 2015;161:49–58.